Journal of the Brazilian Society of Mechanical Sciences and Engineering (2019) 41:124
https://doi.org/10.1007/s40430-019-1621-2

TECHNICAL PAPER

Optimization of process parameters of direct metal laser sintering process using fuzzy-based desirability function approach

Hiren Maganbhai Gajera[1,2] · Komal G. Dave[2] · Veera P. Darji[1] · Kumar Abhishek[3]

Received: 22 May 2018 / Accepted: 2 February 2019 / Published online: 13 February 2019

Abstract
CL50WS material has been mainly used in tooling industries for making die, tool insert, mould or casting die. As the manufacturing of the CL50WS material parts from the DMLS machine differs from the conventional machining process, it is very essential to understand of DMLS behaviour and determine the proper optimal process parameter. Hence, the present study highlights the application of Box–Behnken method (BBD) of response surface methodology with fuzzy-based desirability function approach in order to optimize the multiple process parameters of direct metal laser sintering. The study also focused to investigate the effects of process parameters, viz. the laser power, scanning speed, layer thickness and hatch spacing, on the performance characteristics such as surface roughness, hardness and impact strength for the fabricated specimen using response surface plot. Fuzzy inference system has been applied in order to aggregate the aforementioned performance characteristics into a single objective response, i.e. multi-performance characteristic index. The optimum values of process parameters such as laser power 130 W, scan speed 550 mm/sec, layer thickness 0.03 mm and hatch spacing of 0.010 mm have been observed in the present study.

Keywords ANOVA · FIS · RSM · CL50WS · Surface roughness · Hardness · Impact strength

1 Introduction

The design and manufacturing of dies and mould play a significant role in any production sector. Nowadays, additive manufacturing (AM) is widely accepted by industries for their unique capabilities to produce direct parts from a computer-aided design (CAD) file. Direct metal laser sintering (DMLS) is emerging technology among various rapid prototyping methods [1]. It is one of the AM techniques adapted to produce the three-dimensional parts or functional unit by laser-sintered material layer by layer without using any binder, vibration force or mechanical force. Also, it does not require additional post-processing technology [2]. According to the current market demands, several industries (especially aerospace and tooling) have been forced to reduce the time and to be cost-effective along with the high level of quality. This pressure has forced these industries to optimize the parameters for the better DMLS-fabricated components [3].

Recently, CL50WS has gained immense attraction in the recent years with metallic AM technologies. CL50WS is being used in various sectors as such as tooling industries, aerospace, automotive, medical and other industries. This is possible because of its superficial mechanical characteristic like high strength, high fracture toughness, good weldability at elevated temperatures [4]. Notwithstanding, the mechanical properties of DMLS-made parts do not fully rely on material utilized; they are also affected by the process parameters. With DMLS, numerous process parameters

Technical Editor: Márcio Bacci da Silva, Ph.D.

✉ Hiren Maganbhai Gajera
gajera.hiren684@gmail.com

Komal G. Dave
dave_komal@yahoo.co.in

Veera P. Darji
veera.jani@rediffmail.com

Kumar Abhishek
krabhishek1987@gmail.com; kumarabhishek@iitram.ac.in

[1] Mechanical Engineering, C.U. Shah University, Surendranagar, Wadhwan, Gujarat, India

[2] Mechanical Department, L.D. Engineering College, Ahmedabad, Gujarat 380009, India

[3] Mechanical Department, IITRAM, Ahmedabad, Gujarat, India

affect the surface quality and mechanical property of parts, including the laser power, scanning speed, layer thickness and hatch spacing as shown in Fig. 1.

Yasa et al. [4] analysed the effect of the SLM parameters (scan speed and layer thickness) on the density, surface quality and hardness of maraging steel 300 parts. It has been observed that heat treatment for 5 h at 480 °C provides high hardness within a relatively short time. It has been also found that SLM 18 Ni maraging steel possesses more tensile strength than wrought 18 Ni maraging steel. Similar results have found for similar material by Kempen et al. [6]. Benedetti et al. [7] have reported surface roughness of built specimen is 7 µm which can even be reduced by post-treatment. The crack initialization and crack propagations lead to corrosion fatigue failure of AlSi10 Mg alloy [8]. Mengucci et al. [8, 9] have reported a lot of work on manufacturing of bio-metals using DMLS. The average value of the surface roughness was 2.2 µm and 6.69 µm for Co–Cr–Mo–W and Ti–6Al–4V alloy, respectively, made by DMLS. They have found that laser power, scan speed and orientation are the prime parameters for the variation in the surface roughness of parts. Pal et al. [9] have reported the effect of process parameters like laser power (150–195 W) and scan speed (700–900 mm/s) on the surface roughness of stainless steel PH1 alloy. They have revealed that minimum surface roughness (9.39–10 µm) was obtained at laser power 150 W and scan speed 900 mm/s. The surface roughness does not rely on the orientation [10]. Chaolin Tan et al. [11] have measured the surface roughness for the even surfaces and the vertical surfaces for the high-performance grade 300 maraging steels. They have seen that the hardness, tensile strengths and ductility of as-fabricated and solution-aged SLM-made specimens is reached to the standard wrought material. Casalino et al. [12] have investigated the effect of laser power (57 W, 86 W, 100 W) and scan speed (180 mm/s, 200 mm/s, 220 mm/s) on surface roughness, ultimate tensile strength (UTS) and hardness of 18 Ni 300 maraging steel. The laser power greater than 90 W and the speed less than 220 mm/s enhance the part properties (UTS and hardness). AlMangour et al. [13] have investigated the effect of shot peening on surface roughness. They have concluded that low-cost shot-peening treatment is very effective to reduce the surface roughness of an untreated sample. Yasa et al. [14] have investigated the effect of variation of inclination angle on the surface roughness of impeller part. They have suggested that the large inclination angle reduces surface roughness. Hermann et al. [15] have reported that tensile strength of maraging 18 Ni 300 steel decreases at high hatch space. Moreover, the tensile properties do not rely on building orientation. The high density was found at the hatch spacing of 0.7d (where d is laser beam diameter), laser speed of 600 mm/s and double scanning pattern. Ferreira et al. [16] has concluded that high porosity (%), lower tensile strength and lower stiffness were obtained at the higher scan speed (400 or 600 mm/s) for the hybrid material of steel (hot work steel and SS AISI 420). Suryawanshi et al. [17] have revealed

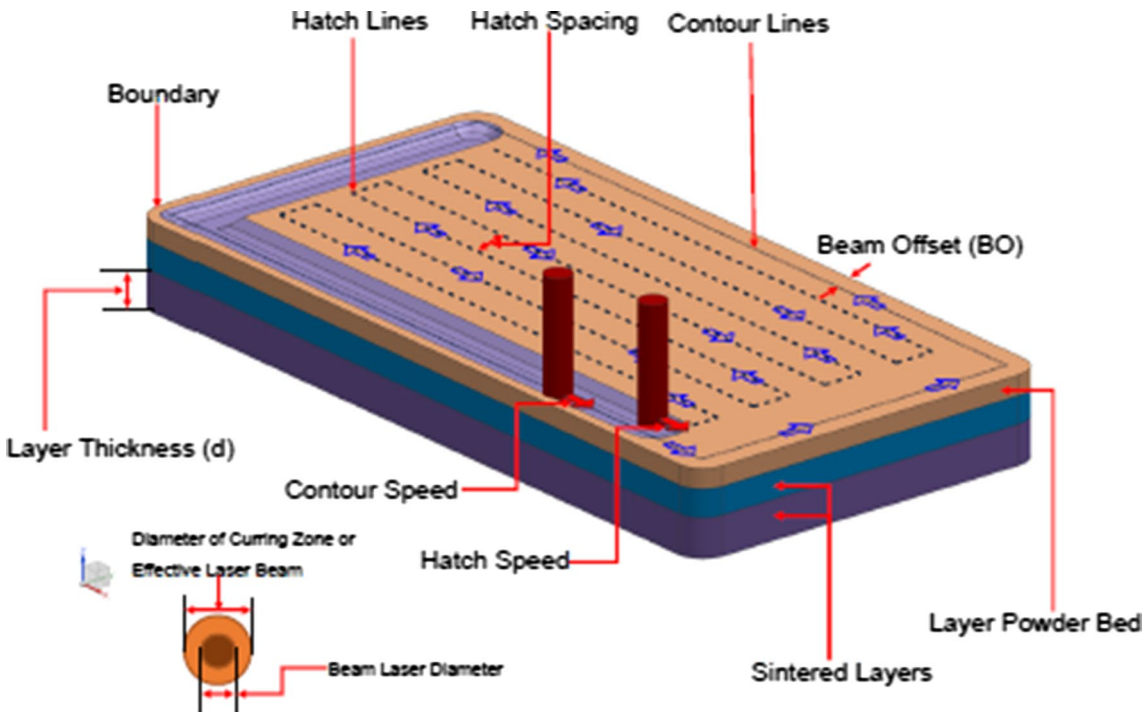

Fig. 1 Exposure strategies and process parameters [5]

that mechanical properties of SLM-made parts do not influence by anisotropy. Sanz et al. [18] have investigated the effect of post-processing (shot peening and surface cleaning) on mechanical properties of maraging steel, Inconel 718 and CoCr alloy. They have found that the hardness of specimen increases in the centre of the specimen after heat treatment. Cajner et al. [19] have said that plasma nitriding process has improved wear resistance of maraging steel. Bai et al. [20] have seen that micro-hardness of the top surface is nearly the same as the side face of part after conducting various heat treatments of SLM-made maraging steel material. They inferred that impact strength is definitely reduced after solutionizing and ageing treatment.

Krishnan et al. [21] have reported that laser power of 180 W, scan speed of 700 mm/s and hatching spacing of 0.1 mm were noteworthy for the superior hardness of AlSi10 Mg parts. They have concluded that hatching distance is the most affecting parameter for the hardness. Yadollahi et al. [22] have revealed that fatigue life can be improved by reducing the stress level in part while conducting heat treatment. Conversely, Wang et al. [23] have manufactured specimen with lower linear heat input (laser power (2300 W), travel speed (8.5 mm/s), layer thickness (0.8 mm)) and higher heat input (laser power of 4000 W, travel speed of 10.6 mm/s and layer thickness of 1.2 mm) for stainless steel 304 material. The result had said that good mechanical properties and microstructure are attained at the lower heat input. Guan et al., [24] have investigated the effect of layer thickness (20 µm, 30 µm and 40 µm), overlapping rate (0%, 10%, 20%, 30% and 40%), part building orientation (00, 450 and 900) and hatch angle (90°,105°,120° and 135°) on tensile properties of SLM-made stainless steel 304 material parts. They have seen that the good tensile properties are attained at a hatch angle 105°. Fritz et al. [25] have reviewed the work on laser AM for metallic material for hot work steel. They have found that several works have been explored on Ti–6Al–4V material for biomedical field, while material relating to the die and mould making industries has not been investigated till date. Kumar et al. [26] and Hussain et al. [27] have investigated the hardness of DMLS-made parts.

Most of the research has been done for technological improvement, post-treatment on AM-made parts and finding the behaviour of heat-treated parts. It has been evident from the existing literature that limited work has been carried in order to investigate the effect of process parameters on surface roughness for CL50WS material. It is also apparent from the literature [4–27] that there has been no systematic or efficient investigation carried out for the application of the CL50WS material. The individual and combined effects of the distinctive parameters on the hardness, surface quality and impact strength of DMLS parts are presently ineffectively comprehended. In addition, optimization of more than one responses of the DMLS process for CL50WS material has not been studied very well till date. The literature does not provide a suggestion for the experimenter to choose the best optimal parameter setting for the aforesaid responses for the CL50WS material. Hence, it is very essential to determine the optimal parameter setting for the aforesaid responses of a CL50WS material.

This study useful for those industries that are using DMLS-made die or mould. The dimensional accuracy of DMLS-fabricated parts is seriously affected by the surface roughness. Moreover, the high hardness and high amount of toughness must be required in the material of die or mould to sustain the uncertain forces during the operation of the die. Hence, it is very essential to optimize the process parameter of DMLS for the surface roughness, hardness and impact strength. Hence, the CL50WS material of DMLS will put the first step for its commercialization and adoption of DMLS technology in die and mould industries.

In this study, individual specific weight has been assigned to the responses. These weights might be changed as per the responses. Generally, these responses do not have the same priority or weight. The intensity of this weight relies on the application area of part and demand of the parts. Generally, the high degree of hardness and toughness is required to sustain high load during processing of die and punch. It is expected that the surface roughness of DMLS-made specimen should be less in order to reduce the post-processing cost and as well as to prevent the dimensional accuracy. Thus, response priority weight can be decided only on based on the judgement of the designer. So, the designer has not set priority weight of response in proper manner which increases the inaccuracy in the solution. To avoid these limitations, fuzzy inferences system (FIS) has been proposed.

Therefore, the design of experiment (DOE) was utilized to collect the data to depict the connection among parameters and aforesaid response. At that point, the analysis of experimental results, the effect of process parameters on aforementioned responses were researched, and additionally, optimized conditions were built up to minimize the surface roughness and maximize the hardness and impact strength utilizing the fuzzy-based desirability function approach.

2 Materials and methods

2.1 Material

CL50WS material has been chosen, due to its lack of erosion or splitting issue thanks to high nickel content and less carbon content, which gives great corrosion resistance and wear resistance [4]. The chemical composition of CL50WS (was estimated according to the ASTM E-1086-2014 utilizing spectro-analysis) is shown in Table 1, the

Table 1 Chemical composition (wt %) of base materials

Material	Carbon	Sulphur	Phosphorous	Manganese	Nickel	Chromium	Molybdenum	Copper	Iron
CL 50 WS	0.03	0.010	0.010	0.15	17–19	0.25	4.50–5.20	8.50–10.0	Balanced

Fig. 2 Direct metal laser sintering machine

Fig. 3 DMLS-made specimen

material composition which is very close to maraging steel 18Ni300. The base material in the present research work is CL50WS in the form of powder material.

The specimens were manufactured by using DMLS technique on SLM machine (M1 Cusing model; manufactured by Concept Laser Company) as shown in Fig. 2. The set-up consists of a Ytterbium (Yb) fibre laser system (peak power 200 W) and an inert gas chamber. The DMLS machine having built volume $250 \times 250 \times 250$ mm (x, y, z) uses a fibre laser and melts the powder material into the solid specimen using an intense laser beam. The working chamber provided a closed environment that was filled with nitrogen as a protective gas to maintain an oxygen concentration of 1.8% with the maximum laser power of 200 W, a maximum scanning speed 7 m/sec, a laser beam diameter of 0.03 mm and layer thickness from 0.02 to 0.08 mm. Generally, hatch spacing has been provided by the multiplication of laser beam diameter (hatch spacing = d*value, where d = laser beam diameter). The specimens were prepared on H13 tool steel substrate of 25 mm thickness as shown in Fig. 3. The loading and unloading of substrate load was done from one door, and for powder material, another door was provided in the machine.

2.2 Design of experiment

Design of experiment (DOE) gives a systematic approach to carry out research experiments to determine the best combination of input parameters for achieving a desirable solution for research characteristic.

2.2.1 Response surface methodology

Response surface methodology (RSM) provides a functional relationship between the aforesaid responses and process parameter through the statistical method and analytical method. It is very helpful where such type of relationship models do not exist. In addition, it is a very useful application in such area where conducting experiment trials are very costly and difficult to take a measurement. Generally, the relationship between the responses (Y) and the input parameter (Xi) is unknown, but both are in the relationship through the low-order polynomial model. Box and Wilson have introduced this method in 1951, and they suggested second-order degree polynomials to approximate the relationships as per Eq. 1, although there are other functional forms to apply RSM [28].

$$Y = \beta 0 + \sum_{i=1}^{k} \sum_{i=1}^{k} \beta ixi + \sum_{i=1}^{k} \beta iixi2 + \sum i \sum_{j} \beta ijxixj + e \text{ for } i < j \quad (1)$$

where βi are regression coefficients and xi is the coded variables. In this study, $x1$, $x2$, $x3$ and $x4$ were taken as coded variables. Here, $x1$ is coded variable that describes the laser power; $x2$ is the coded variable that describes the scan speed; $x3$ is the coded variable that describes the layer thickness and $x4$ is coded variable that describe the hatch space. In RSM, the actual variable has been converted into the coded variable dimensionless with mean zero and the same spread or standard deviation. The relationship between the coded variable and natural variable is given by following formula [29]

$$= \frac{A - \frac{(H+L)}{2}}{\frac{(H-L)}{2}} \quad (2)$$

where A = actual variable or natural variable (such as laser power, scan speed, layer thickness and hatch space).

H = the value of the high level of respective factor

L = value of the low level of respective factor.

Box–Behnken design (BBD) is a well-known test outline system used to optimize the process parameter. The BBD system has turned out to be a to a great degree important tool, allowing the exact optimum value of experimental parameters to be determined and additionally the likelihood to assess the communication between factors with a decreased number of trail or experiments. In this examination, 27 specimens of CL50WS material were manufactured with different sets of process parameters for optimization. Three levels of four parameters to be specific laser power, layer thickness; hatches distance and scan speed were chosen. In BBD, only three levels of process parameter have been required to run the experiment, and also, there are no points that lie on the vertices of the experimental vicinity. This is the main characteristic of the BBD method [30–33]. In Box–Behnken design, there are fewer design points than central composite designs which are less expensive to run with the same number of factors. Moreover, Box–Behnken designs never include runs where all factors are at their extreme setting, such as all of the low settings, unlike central composite designs.

The laser power, scanning speed and hatch spacing were finalized by the maximum energy density [26]. Energy density is characterized by the relative laser energy per unit area connected to the powder bed surface and is deciding to utilize Eq.

$$\text{Energy density} = \frac{\text{Laser power (watt)}}{\text{Hatch spacing (mm)} * \text{Scanning speed}\left(\frac{\text{mm}}{\text{sec}}\right)} \quad (3)$$

To maximize the energy density, commonly the higher value of the laser power is utilized for delivering less porous metal parts [12]. The laser power is in this way set to 130 W, to examine the interaction effect, and the laser power is decreased to 110 W and 120 W. Machine manufacture has recommended the laser power from 90 to 130 W for the hot tool steel material. But, proper bonding does not occur at 90 W and 100 W; moreover, the component becomes very hard and burns at more than 130 W laser power. In addition, the balling effect has been seen in the pilot experiment while fabricating specimen above 130 W of laser power. Thus, in this study, laser power was selected from 110 to 130 W which is very suitable for the CL50WS material. To guarantee the metallurgical bond between layers, the melt pool depth should be more prominent than one-layer thickness, extending from 1.3 to 3, which is related to a laser power 110–130 Ws and scanning speed 550–650 mm/sec. Concerning scanning speed and hatch spacing, default values for CL50WS are 600 mm/s and 0.015 mm, respectively, individually as per the recommendation of machine tool manufacturers. An expansion of scanning speed and hatch spacing enhances the rate of production, whereas lower values of these two parameters cause an increase of ED. To guarantee the uniform layer fusion, two subsequent layer tracks must be overlaped. It should be 1.5 to 1.6 times larger than the value of hatch space. Subsequently, width-to-height ratio ought to go between 1.7 and 5, which is related to a hatch spacing going from 0.90 to 0.020 mm and layer thickness which has looked over 0.03–0.05 mm because the manufacturer (Concept laser) has been provided with a range of layer thickness between 0.020 and 0.080 mm. The surface roughness of components is very rough when the value of layer thickness exceeds the 0.050 mm. Obviously, rough surface finish has required more post-processing for the final use of components. Build time of component will increase while utilizing the lower value of layer thickness 0.020 mm. Hence, a layer thickness between the 0.03–0.05 mm is very reliable for the build time as well as the surface finishes [34]. The levels of parameters and plan of the experiment (with coded and actual variables) used in this research are shown in Tables 2 and 3, respectively.

2.2.2 Measurement procedure

In this study, mean of three readings was taken as actual reading of surface roughness (by using surface roughness tester—Mitutoyo, Model—SJ 210) for top surface of the specimen. The surface roughness was measured by stylus having tip radius 5 μm and provides 4 mN measuring force during measurement. The measurement direction was taken perpendicular to laser scan direction along Y-axis of the specimen. Sampling length was taken as 10 mm with measuring the speed of 0.75 mm/s and retraction speed 1 mm/sec.

In this investigation, 27 specimens were fabricated as per the ASTM standard E23-16b [35] and were processed using the surface grinder and broaching machine. The dimensions

Table 2 Levels of process parameters

Sr no	Process parameter	Unit	Level 1 (−1)	Level 2 (0)	Level 3 (+1)
1	Laser power	W	110	120	130
2	Scanning speed	mm/s	550	600	650
3	Layer thickness	mm	0.03	0.04	0.05
4	Hatch distance	mm	0.01	0.015	0.02

Table 3 Plan of the experiment

Sr no.	*X1*	*X2*	*X3*	*X4*	Laser power (W)	Scan speed (mm/s)	Layer thickness (mm)	Hatch distance (mm)
	Coded variable				Actual variable			
1	− 1	− 1	0	0	110	550	0.04	0.015
2	1	− 1	0	0	130	550	0.04	0.015
3	− 1	1	0	0	110	650	0.04	0.015
4	1	1	0	0	130	650	0.04	0.015
5	0	0	− 1	− 1	120	600	0.03	0.010
6	0	0	1	− 1	120	600	0.05	0.010
7	0	0	− 1	1	120	600	0.03	0.020
8	0	0	1	1	120	600	0.05	0.020
9	− 1	0	0	− 1	110	600	0.04	0.010
10	1	0	0	− 1	130	600	0.04	0.010
11	− 1	0	0	1	110	600	0.04	0.020
12	1	0	0	1	130	600	0.04	0.020
13	0	− 1	− 1	0	120	550	0.03	0.015
14	0	1	− 1	0	120	650	0.03	0.015
15	0	− 1	1	0	120	550	0.05	0.015
16	0	1	1	0	120	650	0.05	0.015
17	− 1	0	− 1	0	110	600	0.03	0.015
18	1	0	− 1	0	130	600	0.03	0.015
19	− 1	0	1	0	110	600	0.05	0.015
20	1	0	1	0	130	600	0.05	0.015
21	0	− 1	0	− 1	120	550	0.04	0.010
22	0	1	0	− 1	120	650	0.04	0.010
23	0	− 1	0	1	120	550	0.04	0.020
24	0	1	0	1	120	650	0.04	0.020
25	0	0	0	0	120	600	0.04	0.015
26	0	0	0	0	120	600	0.04	0.015
27	0	0	0	0	120	600	0.04	0.015

of the specimen were 55 × 10 × 10 mm. The impact strength was measured by the Charpy impact machine (Model: IT-30). The tests were carried out at the room temperature. Generally, the specimen was tested on the anvil which is made from alloy steel while the pendulum is mounted on an antifriction bearing and latched at the upper side at 150° (impact point).

Hardness estimations were taken according to the ASTM E18-16 [36] at Indus University, Ahmedabad. The macro-scale hardness was estimated by a hardness tester ((Model: VRS-150) at a preload of 10 kg which was set and was applied the 150 kg load Rockwell C scale (HRC) for one min. The hardness was measured at three various points on the specimen and the mean of it was taken as a final value.

The microstructure of the surface of the specimen has been examined by an optical microscope and scanning electron microscope. The specimen was prepared by polishing followed by diamond polishing to attain mirror-type finish. The etchant composition used for revealing the microstructure was 1 gm CuCl2, 25 ml HNO3, 50 ml HCl and 150 ml water.

3 Results and discussion

As discussed in the previous section, the experiments have been carried out as per the various combinations of process parameters shown in Table 3 whose aforesaid responses are processed as shown in Table 4 for further analysis. The interpretation of the results of the statistical analysis is discussed in the succeeding sections.

3.1 Effect of input parameter on surface roughness

There is a significant effect of interact term laser power versus scan speed and laser power versus layer thickness on surface roughness. Figure 4a–f shows the response surface plot for the effect of input parameters on the surface

Table 4 Experimental results

Sr no.	Laser power (W)	Scan speed (mm/s)	Layer thickness (mm)	Hatch distance (mm)	Surface roughness (μm)	Hardness (HRC)	Impact strength (J)
1	110	550	0.04	0.015	13.540	33.74	30.190
2	130	550	0.04	0.015	8.454	30.19	32.160
3	110	650	0.04	0.015	20.214	27.69	24.000
4	130	650	0.04	0.015	10.994	37.60	33.930
5	120	600	0.03	0.010	6.400	36.83	34.960
6	120	600	0.05	0.010	12.250	26.47	22.230
7	120	600	0.03	0.020	10.963	35.17	20.130
8	120	600	0.05	0.020	18.741	22.00	24.130
9	110	600	0.04	0.010	12.210	32.63	25.000
10	130	600	0.04	0.010	11.987	31.67	42.820
11	110	600	0.04	0.020	15.998	28.43	30.040
12	130	600	0.04	0.020	14.857	29.33	25.090
13	120	550	0.03	0.015	8.994	38.93	29.950
14	120	650	0.03	0.015	10.122	37.53	25.550
15	120	550	0.05	0.015	18.654	24.43	22.180
16	120	650	0.05	0.015	15.898	28.53	21.700
17	110	600	0.03	0.015	9.303	36.93	31.860
18	130	600	0.03	0.015	8.419	39.17	31.500
19	110	600	0.05	0.015	15.473	24.53	21.435
20	130	600	0.05	0.015	13.241	27.00	31.150
21	120	550	0.04	0.010	11.751	31.77	31.600
22	120	650	0.04	0.010	12.365	35.97	28.360
23	120	550	0.04	0.020	17.892	30.50	25.500
24	120	650	0.04	0.020	12.368	28.43	21.330
25	120	600	0.04	0.015	14.095	37.53	24.500
26	120	600	0.04	0.015	14.758	36.23	24.700
27	120	600	0.04	0.015	14.645	36.80	24.680

roughness. Figure 4a shows the effect of laser power and scan speed on surface roughness. It can be seen that lower scan speed and high laser power result in a good surface finish, as high laser power induces a high energy density, which provides a proper melting of powder particle rapidly and exerts low surface roughness. Hence, higher laser power attributes to lower surface roughness. While higher scan speed cannot provide enough time to melt and fuse the particle, the surface finish of part diminishes. It is also seen that the laser should be given enough time to melt and fuse particles resulting in a slow cooling rate; hence, low scan speed provides the better surface finish. From Fig. 4b, it can be seen that surface roughness increases with the increasing layer thickness. Lower layer thickness leads to the lesser spreading of powder which requires less effort to melt it, whereas a considerable amount of time would be required to melt a thick layer of powder (high layer thickness) which subsequently increases the residual stress and warpage of parts. Figure 4c presents the effect of laser power and hatch spacing on surface roughness. From the plot, the lower value of hatch spacing gives lower surface roughness. Generally, hatch spacing provides overlapping of current powder layers on previous layer which gives heat-treating effect to the microstructure of the components. In addition, the hatch spacing provides space to relieve air bubble from improper melting and fusion which exists during previous track [13]. It can be said that 0.020 mm of hatch spacing would be provided at uneven temperatures resulting in surface finish reduction. Hence, the air bubble was found to be relieved at the lower value of hatch spacing due to more overlapping between the powder layers. Figure 4d presents the effect of scan speed versus layer thickness. It can be concluded that the lower value of scan speed and layer thickness gives enough time to melt lower amount of powder resulting in lower value of surface roughness. Figure 4e presents the effect scan speed versus hatch spacing. The slower rate of overlapping between layers can be responsible for the slow cooling rate resulting in reduction of surface roughness at the 550 mm/sec of scan speed and 0.010 mm of hatch spacing. Figure 4f presents layer thickness versus hatch spacing,

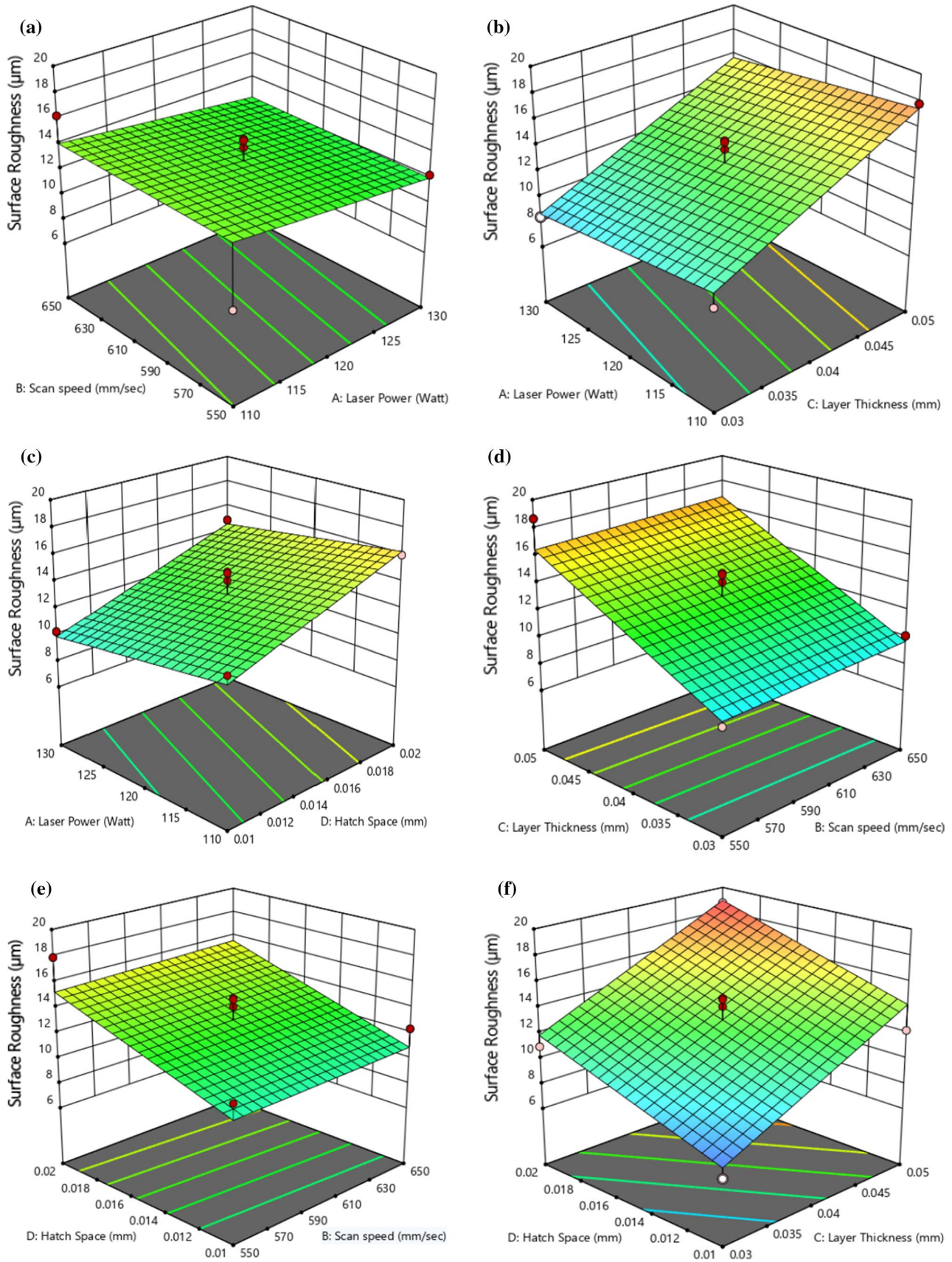

Fig. 4 Response surface plot for surface roughness

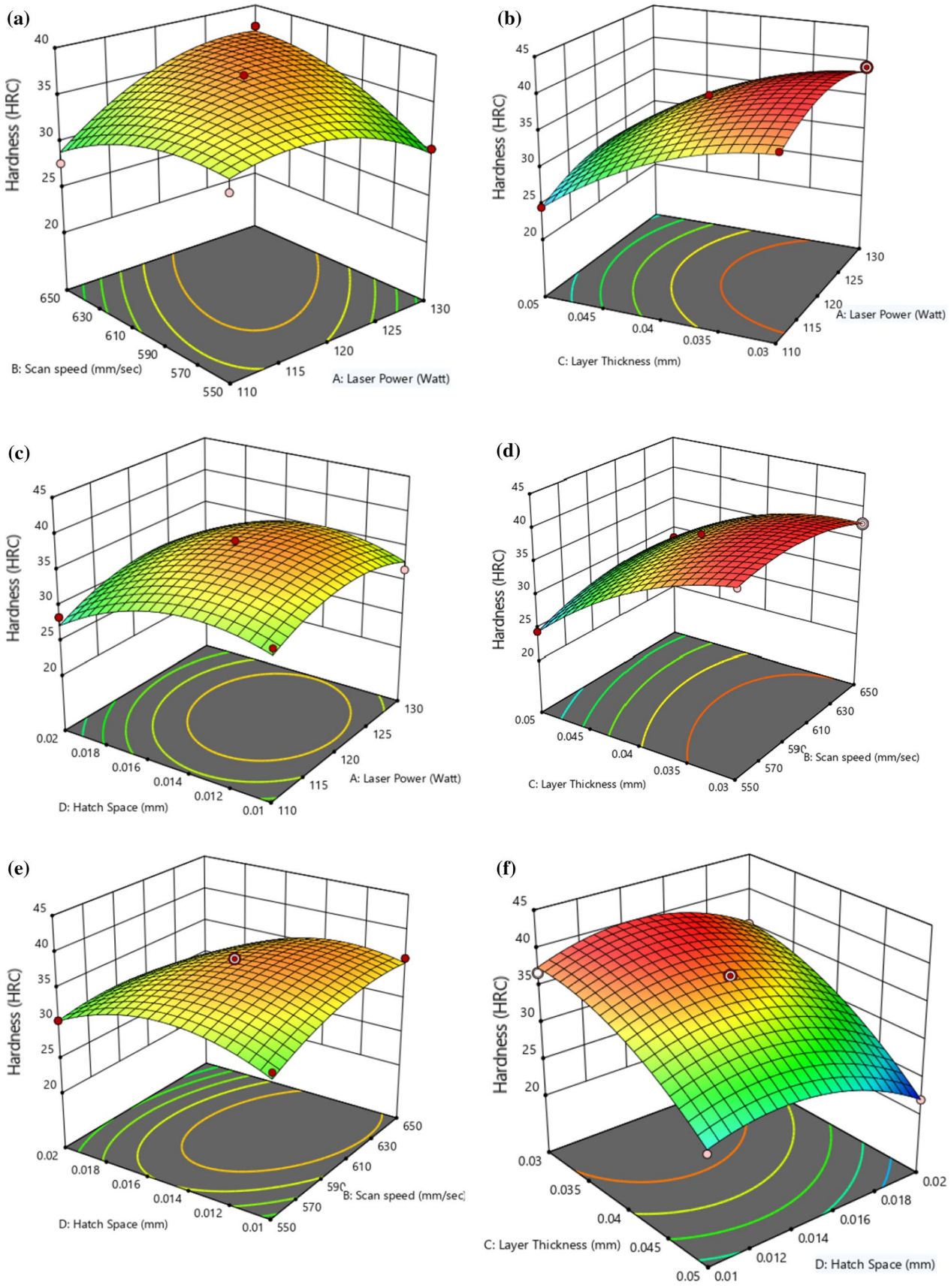

Fig. 5 Response surface plot for hardness

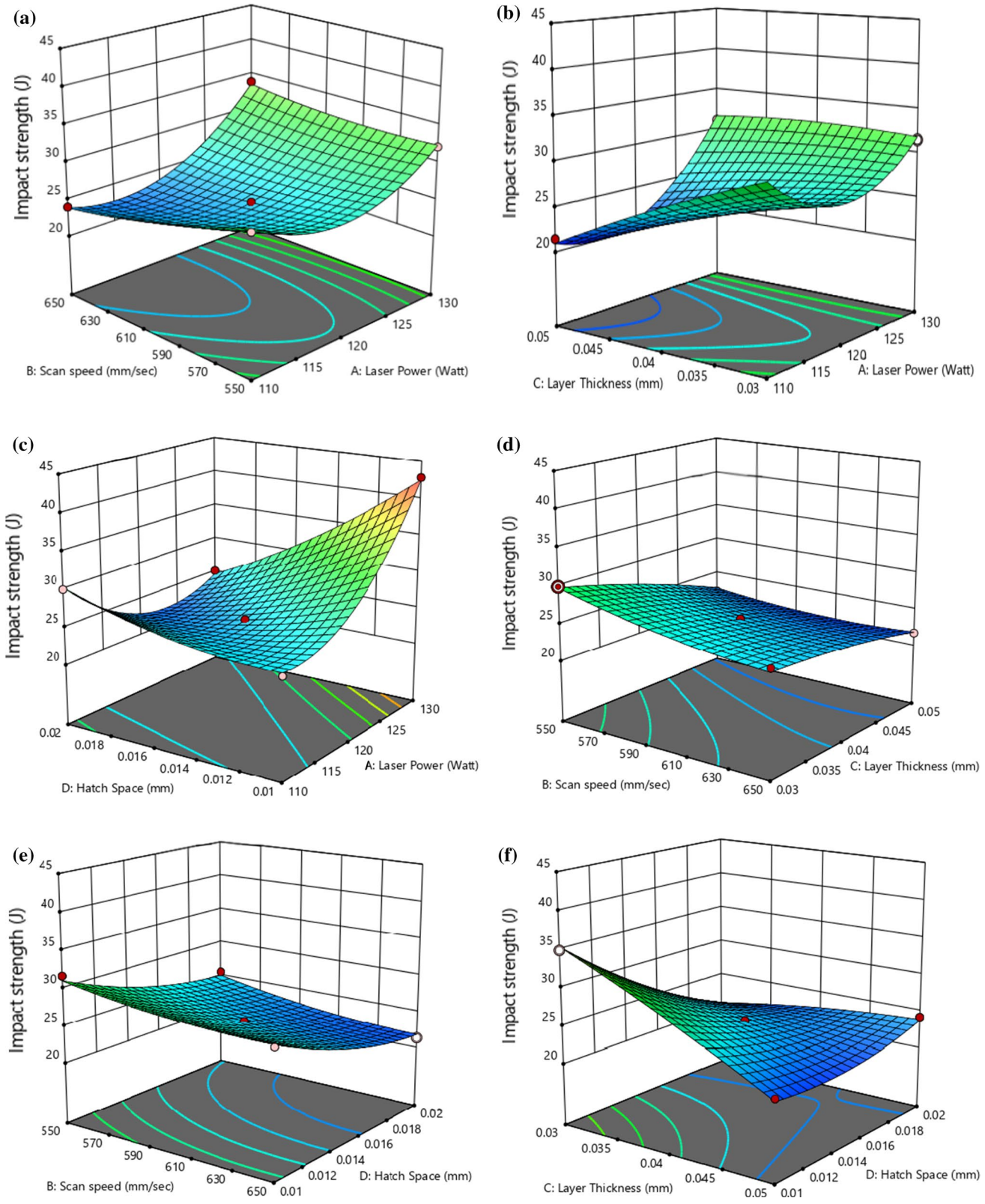

Fig. 6 Response surface plot of impact strength

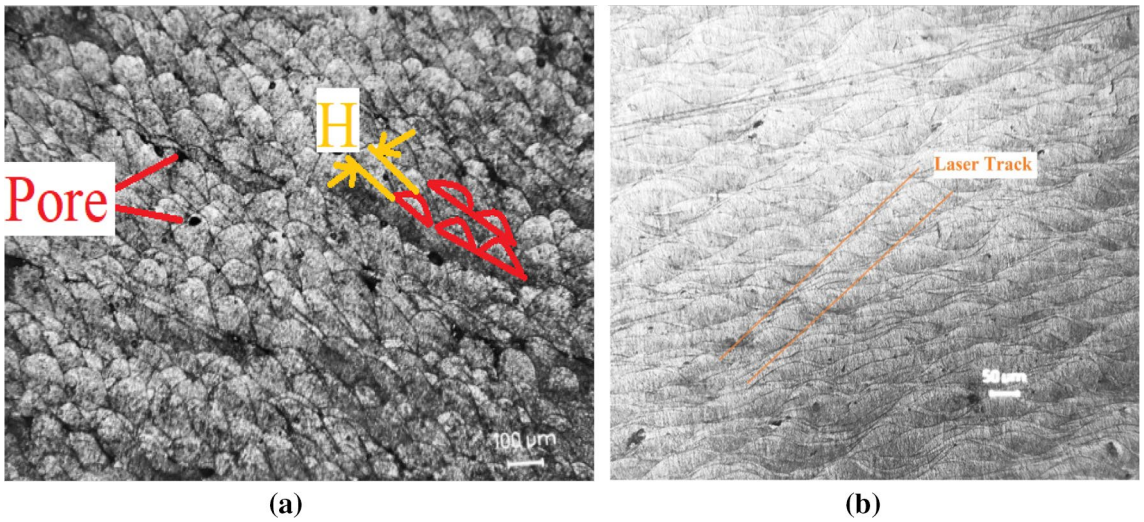

Fig. 7 Optical micrographs of the **a** vertical and **b** horizontal cross sections of the fabricated specimens

where 0.010 mm of hath spacing and 0.030 mm of layer thickness provide slow cooling rate which solidifies all particle homogeneously. Hence, the surface roughness was obtained lesser at the low value of hatch space and layer thickness.

3.2 Effect of input parameter on the hardness

Figure 5a–f presents the response surface plot for input parameter versus hardness. From Fig. 5a, it can be seen that extreme hardness was attained at the value of laser power around 130 Ws and scan speed of around 650 mm/sec. This can be attributed to the fact that high laser power induces high energy which can melt particles rapidly at high temperature making dense homogenous microstructure due to the high cooling rate. Figure 5b represents the effect of laser power and layer thickness on hardness.

It can be also said that the lower layer thickness and high laser power give good hardness as the high laser power gives high energy to generate homogenous structure and does not leave any voids within the scanned layer, whereas low value of layer thickness provides very thin layer which easily gets to melt, making less porous microstructure. Figure 5c gives the effect of laser power and hatch spacing on hardness. Figure 5c shows maximum hardness value at 130 W of laser power and 0.015 mm hatch spacing. It can be seen that lower hatch spacing results in overlapping of the track resulting in relieving of stress and elimination of microscopic segregation. Hence, it is responsible for the good hardness. The effect of layer thickness and scan speed as shown in Fig. 5d suggests that 650 mm/sec of scan speed and 0.03 mm layer thickness result in higher hardness as higher cooling rate attributes to enhanced hardness. Figure 5e and f shows the effect of scan speed versus hatch spacing and layer thickness versus hatch spacing, respectively. The better hardness is obtained at the 550 mm/sec of scan speed and 0.012 mm of hatch spacing as shown in Fig. 5e. The reason is that the microstructure becomes brittle (excessive annealing effect) at the extremely lower (0.010 mm) value of hatch spacing. It can be said that the good hardness is at the 0.03 mm of layer thickness and 0.014 mm of hatch spacing as shown in Fig. 5f. The lower value of layer thickness provides porosity-free dense specimen (finer microstructure) resulting in enhanced hardness.

3.3 Effect of input parameter on impact strength

Figure 6a–f presents the response surface plot for impact strength. Figure 6a presents the effects of laser power and scan speed on impact strength, and it can be said that 130 W of laser power and 550 mm/sec of scan speed give good impact strength. The uniform structure is given by the high intensity of laser power, and lower scan speed makes the structure less porous as well as induces more ductility. Hence, the high value of laser power and low value of scan speed are responsible for the high impact strength.

In addition, it can be said that enough amount of heat conduction has taken place at lower scan speed. Figure 6b presents the effects of laser power and layer thickness for the impact strength. It can be noted that the layer thickness has more influence than the laser power on impact strength. The small amount of powder particle can absorb energy rapidly and make finer structure responsible for the higher strength. Figure 6c presents the effects of laser power and hatch spacing on impact strength. The high value of laser power and low value of hatch spacing lead to high impact strength due

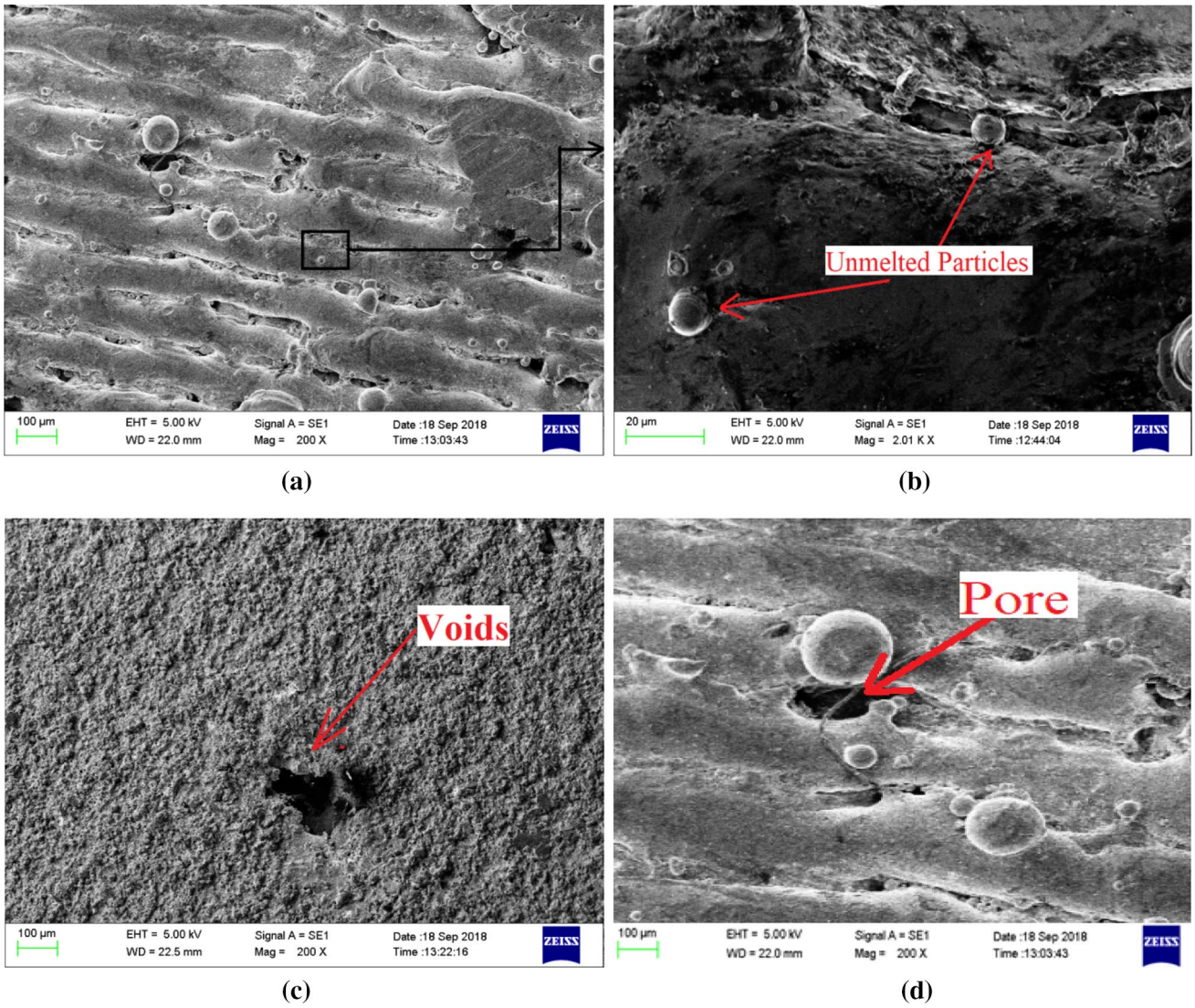

Fig. 8 SEM images of the fabricated specimen

Table 5 Correlation test

Sr. no.	Correlation between	Value of *r*
1	Surface roughness and hardness	−0.658999
2	Surface roughness and impact strength	−0.514342
3	Impact strength and hardness	0.350338

to overlapping which can increase the reheating and produce ductile microstructure, whereas high value of hatch spacing leaves some unmelted powder due to less amount of energy, leading to low relative density and reduction in the strength of the part. Figure 6d represents the effect of scan speed versus layer thickness for impact strength. The toughness of parts increased at the 550 mm/sec of scan speed and 0.03 mm of layer thickness because powder particles are melted at very slow rate (slow cooling rate) resulting in increase in the ductility. The effect of scan speed on the impact strength is not much significant than layer thickness. The effect of scan speed versus hatch spacing for the impact strength is shown in Fig. 6e. It can be said that low value of scan speed and hatch spacing are responsible for the good toughness because of heat-treating effect (remelting of the previous layer particle) which reduces the chance of voids or porosity. The effect of the layer thickness versus hatch spacing for the impact strength is shown in Fig. 6f. The impact strength is found better at 0.05 mm of layer thickness and 0.010 mm of hatch spacing. The microstructure becomes brittle while applying 0.03 mm of layer thickness and 0.010 of hatch spacing on powder bed because of overheating of

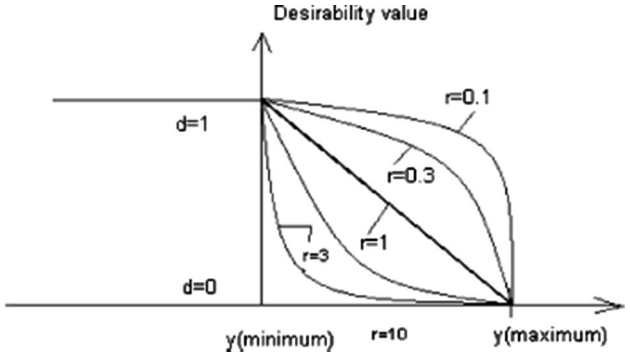

Fig. 9 Desirability function (lower-the-better)

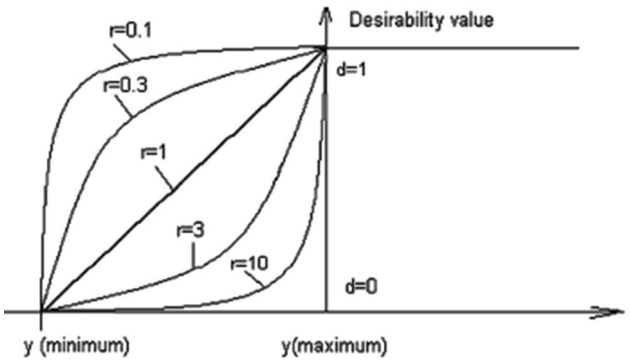

Fig. 10 Desirability function (higher-the-better)

bed. In order to avoid these overheating, 0.05 mm of layer thickness with 0.010 mm of hatch spacing gives enough energy to the powder bed and is capable of filling voids.

3.4 Microstructure

As shown in Fig. 7a, it can be seen that half ellipse looks like fish scales of 30–50 µm in height. It can be assumed that height of fish scales is near to the layer thickness of powder. Here, it can be said that the width of the fish scale is higher due to the laser beam slanting towards the direction of the laser head. Also, the width of the fish scale has been changing throughout the bed because of the temperature difference and consistently changing solidification rate entirely on the powder bed as shown in Fig. 7b. The flat cross-area (horizontal) shows the movement tracks of laser head over the bed. The width of the track is around 40–45 µm approximately, which is marginally higher than the laser beam diameters (around 30 µm). Subsequently, it unmistakably mirrors the profile of the laser liquid pool. Also, some micro-pores have been visible at higher magnification shown in Fig. 7a which is clearly depicting that mean size of the micro-pores is around 15–20 µm.

Table 6 Individual desirability value of the responses and MPCI

Sr no.	Individual desirability			MPCI
	Surface roughness	Hardness	Impact strength	
1	0.482983	0.683751	0.443367	0.689
2	0.851267	0.476995	0.53019	0.733
3	0	0.331392	0.17056	0.326
4	0.667343	0.908561	0.608197	0.765
5	1	0.863716	0.653592	0.82
6	0.576394	0.260338	0.092552	0.439
7	0.669587	0.767036	0	0.601
8	0.106372	0	0.176289	0.278
9	0.57929	0.619103	0.214632	0.615
10	0.595438	0.563192	1	0.755
11	0.304996	0.37449	0.436756	0.56
12	0.387618	0.426907	0.218599	0.537
13	0.812165	0.986022	0.43279	0.743
14	0.730485	0.904485	0.238872	0.65
15	0.112672	0.141526	0.090348	0.363
16	0.312238	0.380315	0.069193	0.435
17	0.78979	0.86954	0.516968	0.794
18	0.853802	1	0.501102	0.817
19	0.343012	0.14735	0.057514	0.362
20	0.504634	0.291206	0.485677	0.63
21	0.612527	0.569016	0.505509	0.753
22	0.568067	0.813628	0.362715	0.671
23	0.167849	0.49505	0.236668	0.467
24	0.567849	0.37449	0.052887	0.472
25	0.442795	0.904485	0.192596	0.562
26	0.394786	0.828771	0.20141	0.539
27	0.402969	0.861969	0.200529	0.543

Generally, the grain growth has been made through two mechanisms. First is expanding the boundary of grains (movement of grain boundary) due to increasing the size of the grains and the second is combining the tiny particles (merging of the sub-grains) with bigger sub-grains. This is the way sub-grains become larger and make microstructure more dense.

In addition, it can be said that the high temperature of the laser is responsible to avoid abnormal grain growth and coarser microstructure. Hence, the strength of the DMLS-made specimen having better than the conventional ones. In this attempt, laser power plays a very crucial role in grain growth (clubbing of the tiny particles with large particles) and reducing the porosity. From the results, it can be said that laser energy density is playing a dominant role in grain growth.

The higher temperature of the laser beam at the centre of the laser beams is responsible for creating the cellular crystal structure and extended acicular structure. In addition, the fine cellular-dendritic structure has been developed due

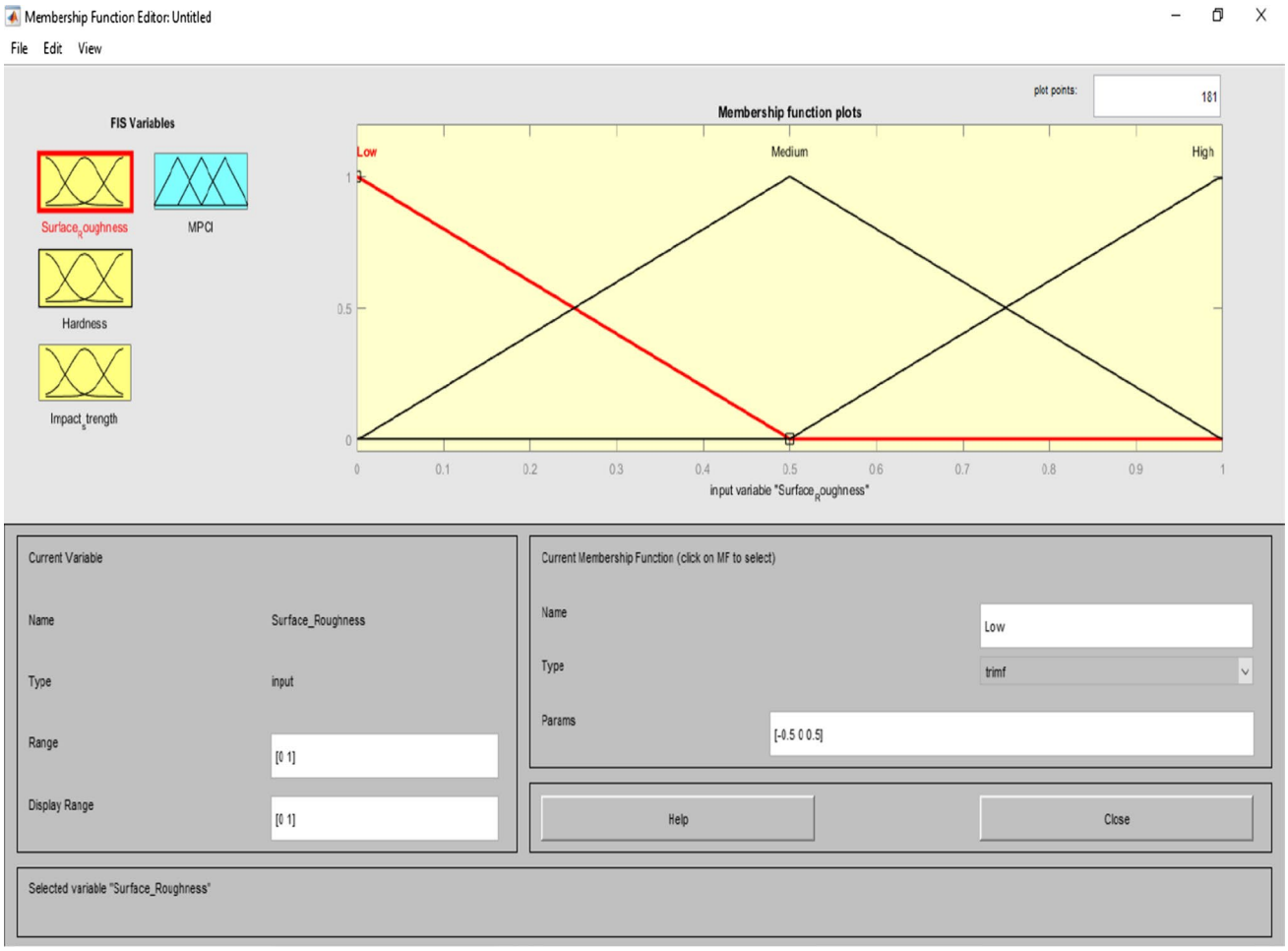

Fig. 11 Membership function (MFs) of desirability value of surface roughness

to the rapid solidification [37]. The similar argument was claimed by the Casalino that high cooling rate is responsible for the finer and cellular microstructure.

The temperature or heat energy of the centre of melt pool (laser beam) is substantially higher than the boundary of the melt pool. The heat has been transferred from the inside to edge because of the heat dissemination. The high scattering rate and high cooling rate are due to the temperature of the melt pool that has stayed under the melting point (Tm) in the centre region. Hence, the level of undercooling ($\Delta T = \mathrm{Tm} - T\mathrm{l}$) is sufficient for new grains nucleation. Henceforth, the liquid metal will encounter haphazardly orientated and synchronous nucleation. In addition, the growth rates of crystal nucleation are very consistent in each direction. Thus, it can be said that equi-axial crystals are effortlessly formed, indicating the microstructure difference of the as-created and heat-treated specimen. In the island scanning strategy, 5 mm × 5 mm square has been scanned by the laser head. Generally, the edge of the boundary or melt pool is rapidly solidified and cooling rate is decreased constantly towards the centre of melt pool. As shown in Fig. 8a, the laser track of island pattern can be easily seen where unmelted particles have been left between the subsequent laser tracks. The ε-phase is developed with transformation of $\gamma \rightarrow \varepsilon$ during the powder bed cooled from the peak temperature. This γ phase exists in powder bed while high thermal gradient results in the unmelted particle in island pattern [38].

Usually, these unmelted particles are found at the boundaries of the laser track as seen in Fig. 8b. As shown in Fig. 8c and d, the development of porosity near about the pool boundaries can be seen. The pore which is developed because of homogeneity does not maintain the melt pool and temperature difference. Then, repeating the cycle of heating and cooling between previous layer and deposited current layer is responsible for the grain morphology. In addition, the fine microstructure (cell spacing, interdendritic space, size of dendrites, etc.) has been found at high cooling rates in

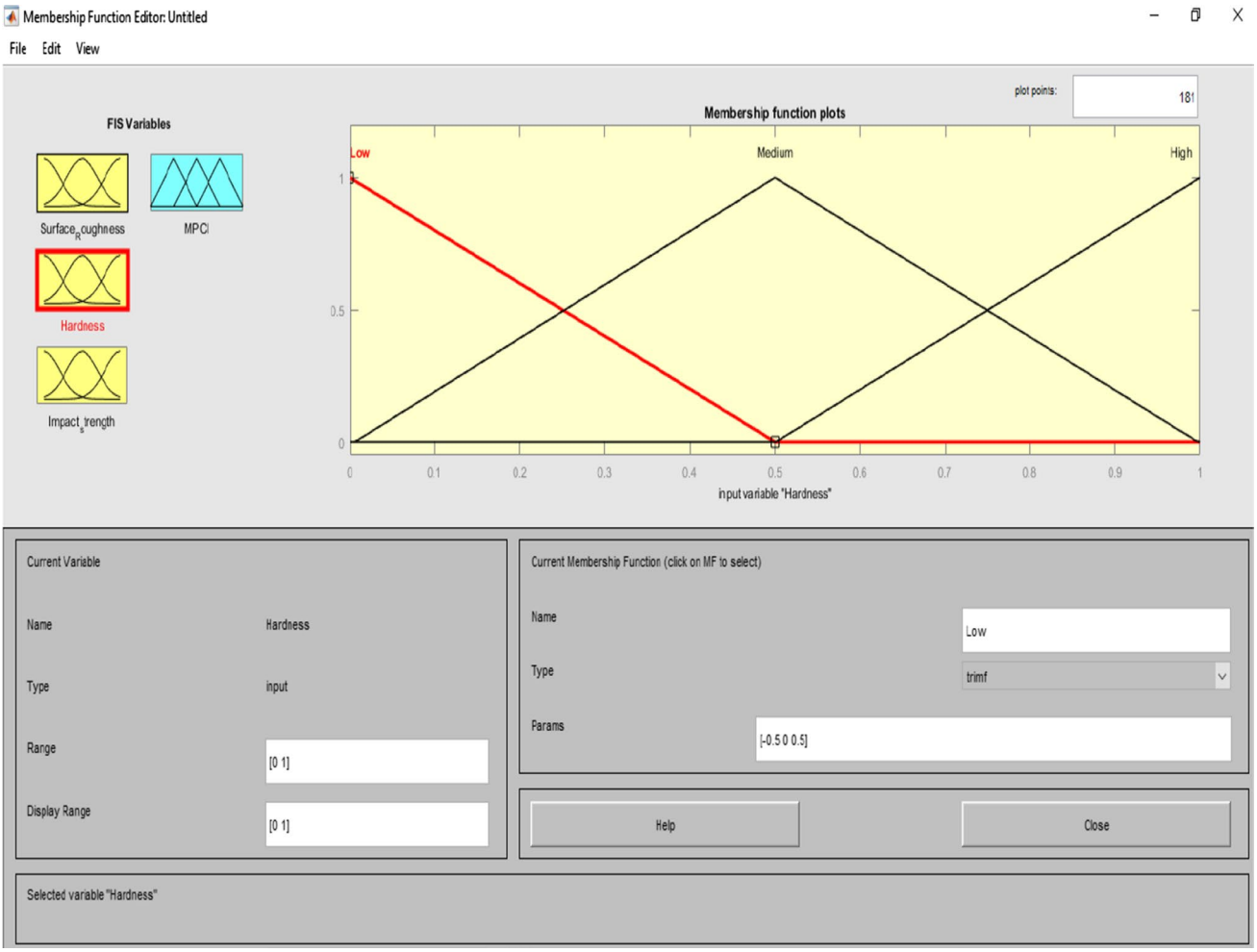

Fig. 12 Membership function (MFs) of desirability value of hardness

DMLS process. These similar results are given by [38–40]. As temperature decreases, crystallization mode changes from planar to cellular, cellular-dendritic and, finally, dendritic solidification mode can be observed [39].

3.5 Correlation of response

In order to check the correlation between the response (i.e. surface roughness, hardness and impact strength), the correlation test has been conducted. Here, the correlation test is shown in Table 5.

4 Optimization method

4.1 Desirability function approach [41]

Derringer and Suich (1980) show the multiple objective optimization methods known as desirability function approach (DFA). DFA is an alluring technique for application of industries problem; especially, it is very suitable and helpful for multiple response optimization of industrial problem. At the initial stage, all individual responses are converted into desirability values. The value of desirability relies on acceptable threshold vicinity as well as the desirable value of the response. The value of desirability is assigned as one while the value of response attains the desirable value, and the value of desirability is assigned as zero while the value of response falls beyond the specified threshold value. Hence, the desirability always lies between the 0–1.

For surface roughness, lower-the-better criterion (as shown in Fig. 9) has been selected for this study. Here, a desirable value of $\bar{I}$ is to be the lower-the-better. The desirability value *di* equals to one while the value of $\bar{I}$ is decreased specific threshold value. If the value of $\bar{I}$ is increased specific threshold value, the value of desirability becomes the zero. Thus, if the value of $\bar{I}$ is falling between the lower threshold value and the upper threshold value, *di* falls between 0 and

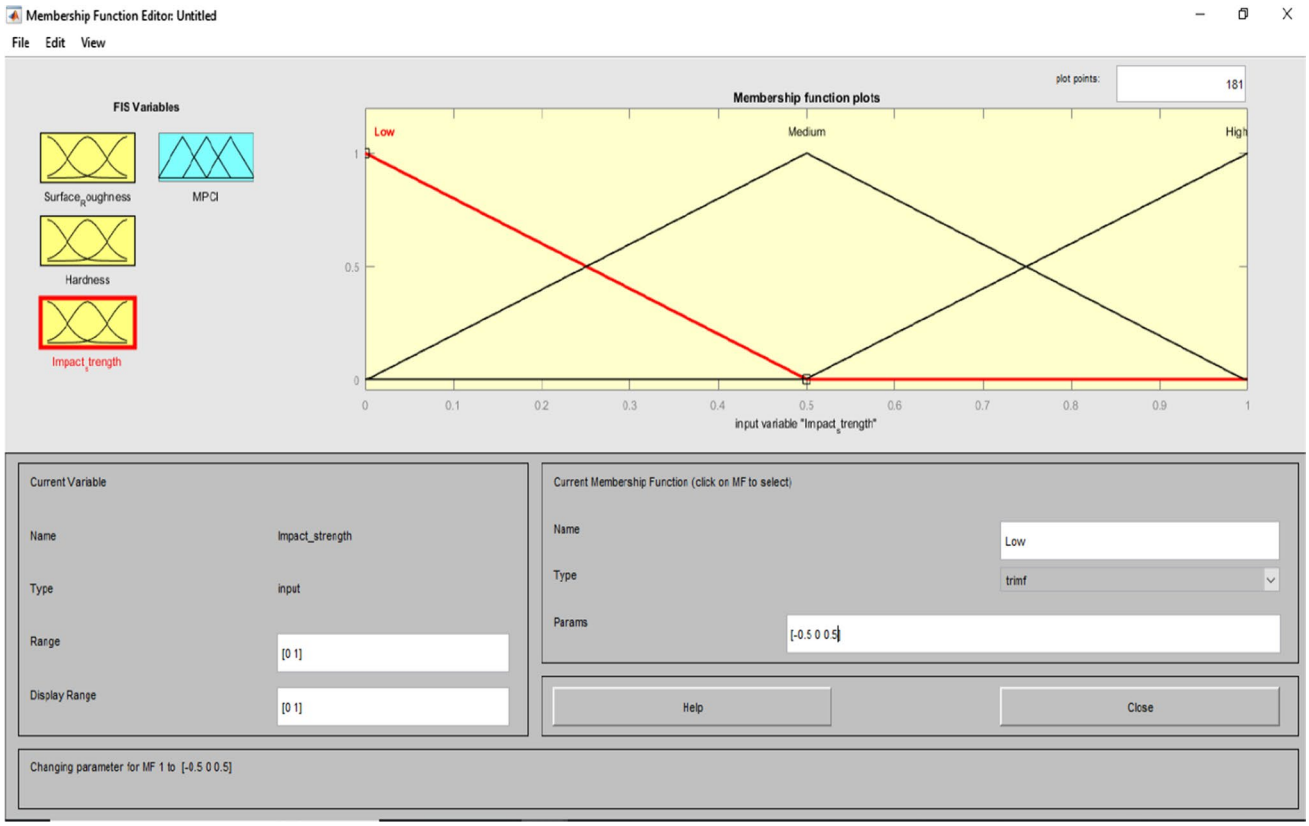

Fig. 13 Membership function (MFs) of desirability value of impact strength

1. Equation no. 4 describes the desirability function of the lower-the-better (LB).

Here,

$$\begin{aligned} &\text{If } \bar{I} \le I_{\min}, d_i = 1 \\ &\text{If } I_{\min} \le \bar{I} \le I_{\max}, di = \left(\frac{\bar{I} - I_{\max}}{I_{\min} - I_{\max}}\right)^r \\ &\text{If } \bar{I} \ge I_{\max}, di = 0 \end{aligned} \tag{4}$$

where I_{min} = The lower threshold limit of $\bar{I}$, I_{max} = The upper threshold limit of $\bar{I}$ and r = The desirability function index

For the hardness and impact strength, the higher-the-better (HB) criterion is selected (as shown in Fig. 10) in this study. In this criterion, the value of $\bar{I}$ is desirable to be the increased. The value of the desirability *di* becomes one while the value of $\bar{I}$ increased beyond the specific threshold value and *di* becomes zero while the value of $\bar{I}$ *is* less than a specific threshold value. Equation 5 represents the desirability function of the higher-the-better (HB) criterion.

$$\begin{aligned} &\text{If} \bar{I} \le I_{\min}, d_i = 0 \\ &\text{If} I_{\min} \le \bar{I} \le I_{\max}, di = \left(\frac{\bar{I} - I_{\min}}{I_{\max} - I_{\min}}\right)^r \\ &\text{If} \bar{I} \ge I_{\max}, di = 1 \end{aligned} \tag{5}$$

In order to calculate the overall desirability, all the individual desirability values have been summation as per Eq. 6.

$$Do = \left(d1^{w1} d2^{w2} d3^{w3} \ldots dn^{wn}\right)^{1/\sum wi} \tag{6}$$

where D_O = The overall desirability value; di = The individual desirability value of *i*th performance characteristic; n = The total number of responses; and Wi = The weight for *i*th attribute.

Here, the sum of all response's weights should be equal to 1. For optimization of process parameters, all individual response goals have been assigned and goal of the process parameter is set to keep in range. The individual desirability of each response combines together and makes

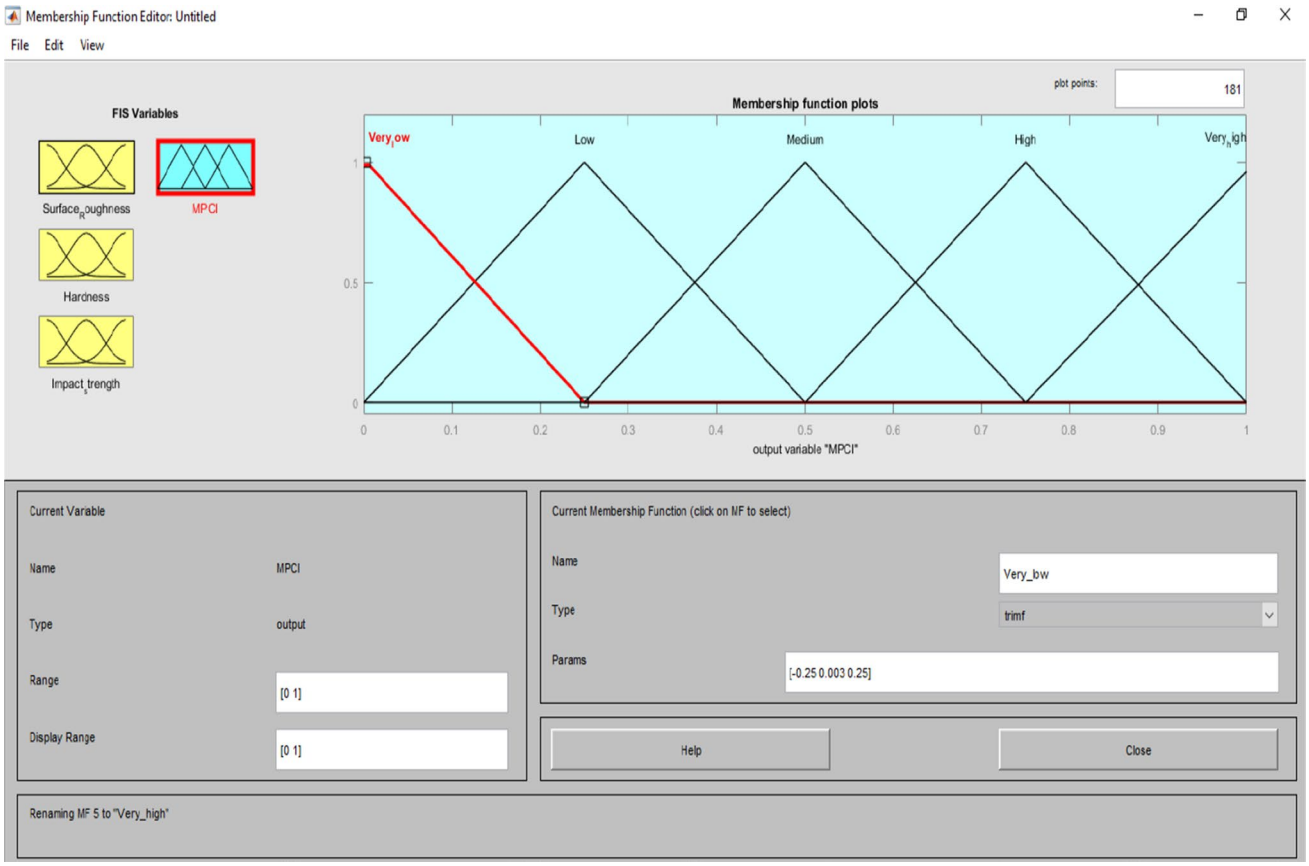

Fig. 14 Membership function (MFs) of MPCI

composite desirability in order to carry out the multi-objective optimization.

4.2 Fuzzy inference system

A fuzzy rule-based system consists of four parts: knowledge base, fuzzifier, inference engine and defuzzifier. The four parts are described below [41].

4.2.1 Fuzzifier

In FIS, real-world input has been inserted in FIS, and this input called as a crisp. Generally, a fuzzy set is a set without a crisp, clearly defined boundary. It can contain elements with only a partial degree of membership. In the FIS system, the crisp value (real-world input) has been treated as an input parameter to the fuzzifier and these crisp values contain the precise information for the particular parameter. In order to change the value in ranges of 0–1, this precise information of crisp value has been converted into the imprecise information (in form of low, medium and high) through fuzzifier.

4.2.2 Knowledge base

Fuzzy operator and fuzzy set are very signification for the fuzzy logic. The conditional statement has been made through using the if–then statement and inserted to the fuzzy logic. For example, a single fuzzy if–then rule assumes the form

If x is L, then y is $H$where L and H are linguistic values defined by fuzzy sets on the ranges x and y, respectively.

4.2.3 Inference engine

The inference operation has been performed by the decision making input or the inference system. It handles the way in which the rules are combined.

4.2.4 Defuzzifier

In the defuzzification, the fuzzy set is a input parameter and an output parameter is a single number. The rule evaluation has been conducted during the intermediate stage by the fuzziness and it gives the final single number called as an

output parameter. However, the integrated fuzzy set includes a range of output values and so must be defuzzified in order to resolve a single output value from the set. Generally, the most popular defuzzification method is the centroid calculation, which returns the centre of the area under the curve.

4.3 Proposed methodology

Table 6 depicts individual desirability values with respect to each response. In this calculation, the higher-the-better criterion has been chosen for hardness and impact strength, and lower-the-better criterion has been adopted for the surface roughness. Henceforth, the purpose of the analysis is to simultaneously maximize the hardness and impact strength and minimize the surface roughness of specimen. For the proposed study, it is essential to convert all responses into the single response, which is known as single performance characteristics. According to the aforesaid desirability criterion adopted, calculated desirability should always be maximized. After that, FIS has been used to import the individual response desirability values as input and it gives multi-performance characteristic index (MPCI) as output. Thus, aforesaid responses have been taken as inputs to FIS. The single output of the FIS is referred as MPCI which has been taken as multiple performance characteristic indexes. It is not required to determine the relation between the responses; weights to the responses do not need to be assigned because the FIS will be taking care of that.

In the FIS, the membership function of the input parameter (responses), namely surface roughness, hardness and impact strength, is described in Figs. 11, 12 and 13, respectively. As shown in Figs. 11, 12 and 13, three fuzzy sets for each parameter of DMLS parameter low, medium and high have been assigned, and five fuzzy sets had been assigned for the output (MPCI) as shown in Fig. 14, which are very low, low, medium, high and very high.

Here, fuzzy number plays an important role in many application; however, the major problem in the development of the application is the computational complexity. Hence, more attention is needed to simplify arithmetic computation with fuzzy numbers. By restricting the fuzzy number to triangular fuzzy numbers, addition and subtraction become simpler.

Here, the input parameters have been fuzzified into the proper linguistic term, and after that, set 27 logic rules in the FIS, which are shown in Table 7 (as shown in Fig. 15). Here, the construction of the rule base is a crucial and most difficult aspect of the fuzzy system design as there are no systematic tools for forming the rule base. However, based on intuitive knowledge and experience of a personnel closely associated with system process, this allows the introduction of "rule-base thumb" experience in the fuzzy system. Therefore, the strength and quality of rule base depend on how good the process skills are extracted from the personnel.

Table 7 Fuzzy rules matrix

Sr. no.	IF surface roughness &	IF hardness &	IF impact strength &	THEN MPCI
1	Low	Low	Low	Very low
2	Low	Low	Medium	Low
3	Low	Low	High	Medium
4	Low	Medium	Low	Very low
5	Low	Medium	Medium	Low
6	Low	Medium	High	Medium
7	Low	High	Low	Low
8	Low	High	Medium	Low
9	Low	High	High	Medium
10	Medium	Low	Low	Low
11	Medium	Low	Medium	Medium
12	Medium	Low	High	High
13	Medium	Medium	Low	Low
14	Medium	Medium	Medium	Medium
15	Medium	Medium	High	High
16	Medium	High	Low	Medium
17	Medium	High	Medium	Medium
18	Medium	High	High	High
19	High	Low	Low	Medium
20	High	Low	Medium	High
21	High	Low	High	Very high
22	High	Medium	Low	Medium
23	High	Medium	Medium	High
24	High	Medium	High	Very high
25	High	High	Low	High
26	High	High	Medium	High
27	High	High	High	Very high

As shown in Fig. 16, insert the value of the input parameter and get MPCI value (as computed in Table 7). To obtain the fuzzy logic rules, a fuzzy set $\overline{A}$ is represented by a triangular fuzzy number which is defined by the triplet (a, b, c). Membership function $\mu\overline{A}(x)$ is defined as:

$$\forall x, a, b, c \in R$$

$$\mu\bar{A}(x) = 0, \text{if } x < a \text{ else} \left(\frac{x-a}{x-b}\right), \text{if } a \le x \le b \text{ else}$$

$$\left(\frac{c-x}{c-b}\right), \text{if } b \le x \le c \text{ else } 0, \text{if } x > c$$

The Mamdani implication method is employed for the rule definition.

Fig. 15 Fuzzy rules matrix

For a rule, R_i: If x_1 is A_{ti} and x_2 is $A_{ti}\ldots x_s$ is A_{si}, then y_i is Ci, $i = 1, 2, \ldots, M$.

Here, M = Total number of fuzzy rule; $x_j(j = 1, 2\ldots, s)$ = input variable; y_i = output variable and

A_{ij} and C_i = fuzzy sets modelled by membership functions for μ_{Aij} and μ_{ci} (y_i), respectively. The aggregated output for the M rules is:

$$\max\left[\left\{\min\left\{\mu_{A_{1i}}(x_1), \mu_{A_{2i}}(x_2), \ldots, \mu_{A_{si}}(x_s)\right\}\right]\right.$$
$$i = 1, 2, \ldots, M \tag{7}$$

The centre of gravity is very popular and effective method for defuzzifying the fuzzy function. In defuzzification process, the crisp value has been calculated for the final output using the following centre of gravity equation

$$\widehat{y_i} = \frac{\int y_i \mu_{ci}(y_i)\mathrm{d}y}{\int \mu_{ci}(y_i)\mathrm{d}y} \tag{8}$$

The non-fuzzy value $\widehat{y_i}$ is referred to as an MPCI (multi-performance characteristic index). As per the previously discussion, the MPCI should be maximum in order to enhance the response. Then, the defuzzification method by the centre of gravity in (Eq. 8) has been used to calculate the crisp value as the final MPCI's outputs. It is required to set possible combination of input parameters in order to calculate the value of MPCI.

4.4 Response optimization

Response optimizer determines the parametric set that optimizes an individual response or a number of responses using the MINITB17 software. For multiple responses, the requirements for all the responses in the set must be fulfilled. A desirability function translates each response scale to a zero-to-one desirability scale, and all these values are inserted in FIS as input to convert one response MPCI. Most desirable values of the MPCI are unity among all combinations of input in order to determine the optimal process parameter. As shown in Fig. 17, optimal parameter setting is laser power 130 W, scan speed 550 mm/sec, layer thickness 0.03 mm and hatch spacing 0.010 mm.

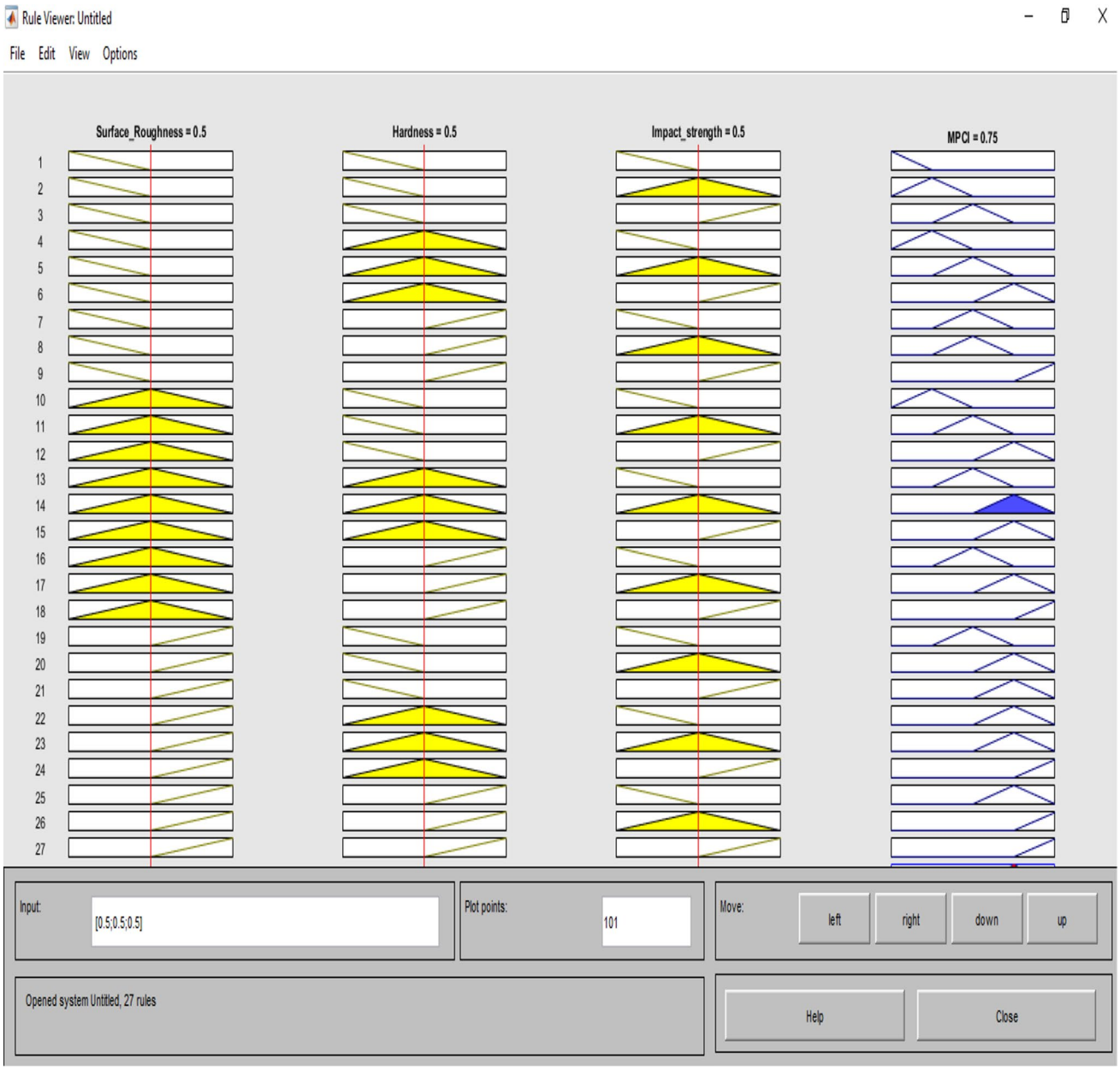

Fig. 16 Membership function (MFs) of MPCI

The value of MPCI (as listed in Table 6) considered as a single response function can be established by the analysis of variance (ANOVA) through MINITAB 17 in order to determine the effect of the process parameter on MPCI (all aforesaid response). The layer thickness, hatch spacing and laser power have been found a significant parameter for the all aforesaid response as shown in Table 8.

5 Conclusion

From the past research, it can be said that the multi-objective optimization problem in case of DMLS-made specimen with the same region of control parameters almost nil to address. The current attempt concentrated to optimize the responses, namely surface roughness, hardness and impact strength of DMLS-made CL50WS material. Box–Behnken method of response surface methodology has been selected to identify the input parameters set to carry out the experiment. Moreover, it is also helpful to reduce the number of runs compared to the central

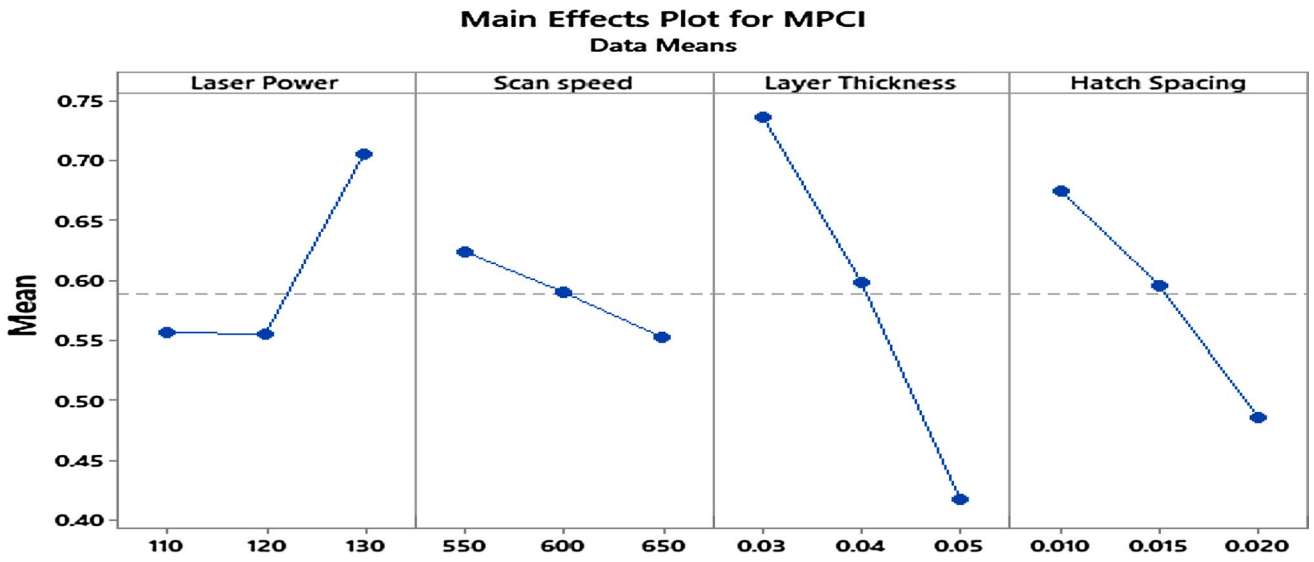

Fig. 17 Evaluation of parametric setting

Table 8 Analysis of variance for MPCI

Source	Degree of freedom	Adj sum of square	Adj mean of square	*F* value	*P* value
Laser power	1	0.066157	0.066157	9.31	0.006
Scan speed	1	0.015337	0.015337	2.16	0.156
Layer thickness	1	0.306560	0.306560	43.13	0.000
Hatch spacing	1	0.107920	0.107920	15.18	0.001

composite design. Fuzzy inferences system has been used to translate three performance characteristics into the one single response called multi-performance characteristic index (MPCI).

1. In this study fuzzy-based desirability function approach, it does not need to assign individual weight to individual response.
2. Based on the ANOVA table of MPCI, it can be said that layer thickness, hatch space and laser power are a significant parameter for all responses in ascending order.
3. From the study, it can be said that optimal parameter setting is laser power 130 W, scan speed 550 mm/sec, layer thickness 0.03 mm and hatch spacing 0.010 mm. The microstructure becomes very dense and finer due to the lower value of the layer thickness. Also, proper melting and bonding occurred at the high value of laser power responsible for increasing the aforesaid response. At the lower value of hatch, space is responsible for the removing air bubble from the previous track through the overlapping of the subsequent layer, thus increasing mechanical properties.

There is some limitation of this work that overheating of subsequent layer causes balling phenomena to occur. The stair case effect of the layer thickness cannot be eliminated, but it can be only minimized to get the good surface finish. Also, the direction of thermal cooling cannot be controlled during the entire part build. There is some performance characteristic of DMLS-made components which still do not explore properly built time, wear rate and dimensional accuracy. This response can be addressed to determine the optimal parameter setting in future work.

References

1. Lee J-H, Jang J-H, Joo B-D, Yim H-S, Moon Y-H (2009) Application of direct laser metal tooling for AISI H13 tool steel. Trans Nonferrous Met Soc China 19:s284–s287
2. Huang SH, Liu P, Mokasdar A, Hou L (2013) Additive manufacturing and its societal impact: a literature review. Int J Adv Manuf Technol 67(5–8):1191–1203
3. Altan T, Lilly B, Yen YC (2001) Manufacturing of dies and molds. CIRP Ann Manuf Technol 50(2):404–422
4. Yasa E, Kempen K, Kruth J (2010) Microstructure and mechanical properties of maraging steel 300 after selective laser melting.

In: Proceedings of 21st international solid freeform fabrication symposium, pp 383–396
5. Bineli RAR, Peres APG, Jardini AL, Maciel Filho R (2011) Direct metal laser sintering (DMLS): technology for design and construction of microreactors. In: 6th Brazilian conference on manufacturing engineering, pp 1–7
6. Kempen K, Yasa E, Thijs L, Kruth JP, Van Humbeeck J (2011) Microstructure and mechanical properties of selective laser melted 18Ni-300 steel. Phys Procedia 12(Part A):255–263. https://doi.org/10.1016/j.phpro.2011.03.033
7. Benedetti M et al (2017) The effect of post-sintering treatments on the fatigue and biological behavior of Ti–6Al–4V ELI parts made by selective laser melting. J Mech Behav Biomed Mater 71(January):295–306
8. Leon A, Aghion E (2017) Effect of surface roughness on corrosion fatigue performance of AlSi10Mg alloy produced by selective laser melting (SLM). Mater Charact 131(2016):188–194
9. Pal S, Tiyyagura HR, Drstvenšek I, Kumar CS (2016) The effect of post-processing and machining process parameters on properties of stainless steel PH1 product produced by direct metal laser sintering. Procedia Eng 149:359–365. https://doi.org/10.1016/j.proeng.2016.06.679
10. Mengucci P et al (2017) Effects of build orientation and element partitioning on microstructure and mechanical properties of biomedical Ti–6Al–4V alloy produced by laser sintering. J Mech Behav Biomed Mater 71(February):1–9
11. Tan C et al (2016) Microstructure and mechanical properties of 18Ni-300 maraging steel fabricated by selective laser melting. In: 6th international conference on advanced design and manufacturing engineering microstructure, 2016, no. ICADME 2016, pp 863–870
12. Casalino G, Campanelli SL, Contuzzi N, Ludovico AD (2015) Experimental investigation and statistical optimisation of the selective laser melting process of a maraging steel. Opt Laser Technol 65:151–158
13. AlMangour B, Yang JM (2016) Improving the surface quality and mechanical properties by shot-peening of 17-4 stainless steel fabricated by additive manufacturing. Mater Des 110(5):914–924
14. Yasa E, Poyraz O, Solakoglu EU, Akbulut G, Oren S (2016) A study on the stair stepping effect in direct metal laser sintering of a nickel-based superalloy. In: Procedia CIRP, 2016
15. Becker TH, Dimitrov D (2016) The achievable mechanical properties of SLM produced Maraging Steel 300 components. Rapid Prototyp J 22(3):487–494
16. Ferreira JAM, Santos LMS, da Silva J, Costa JM, Capela C (2016) Assessment of the fatigue life on functional hybrid laser sintering steel components. Procedia Struct Integr 1:126–133. https://doi.org/10.1016/j.prostr.2016.02.018
17. Suryawanshi J, Prashanth KG, Ramamurty U (2017) Tensile, fracture, and fatigue crack growth properties of a 3D printed maraging steel through selective laser melting. J Alloys Compd 725(25):355–364. https://doi.org/10.1016/j.jallcom.2017.07.177
18. Sanz C, García Navas V (2013) Structural integrity of direct metal laser sintered parts subjected to thermal and finishing treatments. J Mater Process Technol 213(12):2126–2136. https://doi.org/10.1016/j.jmatprotec.2013.06.013
19. Cajner F, Landek D, Leskov V (2010) Surface modifications of maraging steels used in the manufacture of moulds and dies. J Mater Technol 44:85–91
20. Bai Y, Yang Y, Wang D, Zhang M (2017) Influence mechanism of parameters process and mechanical properties evolution mechanism of maraging steel 300 by selective laser melting. Mater Sci Eng A 703:116–123. https://doi.org/10.1016/j.msea.2017.06.033
21. Krishnan M et al (2014) On the effect of process parameters on properties of AlSi10Mg parts produced by DMLS. Rapid Prototyp J 20(6):449–458
22. Yadollahi A, Shamsaei N, Thompson SM, Elwany A, Bian L (2017) Effects of building orientation and heat treatment on fatigue behavior of selective laser melted 17-4 PH stainless steel. Int J Fatigue 94:218–235
23. Wang Z, Palmer TA, Beese AM (2016) Effect of processing parameters on microstructure and tensile properties of austenitic stainless steel 304L made by directed energy deposition additive manufacturing. Acta Mater 110:226–235. https://doi.org/10.1016/j.actamat.2016.03.019
24. Guan K, Wang Z, Gao M, Li X, Zeng X (2013) Effects of processing parameters on tensile properties of selective laser melted 304 stainless steel. Mater Des 50:581–586. https://doi.org/10.1016/j.matdes.2013.03.056
25. Klocke F, Arntz K, Teli M, Winands K, Wegener M, Oliari S (2017) State-of-the-art laser additive manufacturing for hot-work tool steels. Procedia CIRP 63:58–63
26. Kumar N, Kumar H, Khurmi JS (2016) Experimental investigation of process parameters for rapid prototyping technique (selective laser sintering) to enhance the part quality of prototype by Taguchi method. Procedia Technol 23:352–360. https://doi.org/10.1016/j.protcy.2016.03.037
27. Hussain M, Mandal V, Kumar V, Das AK, Ghosh SK (2017) Development of TiN particulates reinforced SS316 based metal matrix composite by direct metal laser sintering technique and its characterization. Opt Laser Technol 97:46–59
28. Kirboga S, Öner M (2013) Application of experimental design for the precipitation of calcium carbonate in the presence of biopolymer. Powder Technol 249:95–104. https://doi.org/10.1016/j.powtec.2013.07.015
29. Myers RH, Montgomery DC, Anderson-Cook CM (2009) Response Surface Methodology: Process and Product Optimization Using Designed Experiments. John Wiley and Sons, Hoboken
30. Esakki B, Rajamani D, Arunkumar P (2017) Modeling and prediction of optimal process parameters in wear behaviour of selective inhibition sintered high density polyethylene parts. Prog Addit Manuf 3:109–121
31. Khajeh M (2009) Application of Box-Behnken design in the optimization of a magnetic nanoparticle procedure for zinc determination in analytical samples by inductively coupled plasma optical emission spectrometry. J Hazard Mater 172(1):385–389. https://doi.org/10.1016/j.jhazmat.2009.07.025
32. Martinez-Conesa EJ, Egea JA, Miguel V, Toledo C, Meseguer-Valdenebro JL (2017) Optimization of geometric parameters in a welded joint through response surface methodology. Constr Build Mater 154:105–114
33. Kirboga S, Öner M (2017) Investigating the effect of ultrasonic irradiation on synthesis of calcium carbonate using Box–Behnken experimental design. Powder Technol 308:442–450
34. Letenneur M, Brailovski V, Kreitcberg A, Paserin V, Bailon-Poujol I (2017) Laser powder bed fusion of water-atomized iron-based powders: process optimization. J Manuf Mater Process 1(2):23. https://doi.org/10.3390/jmmp10200232017
35. ASTM (2016) ASTM E23-16b: standard test methods for notched bar impact testing of metallic materials. ASTM B Stand i:1–26
36. ASTM E18-15 (2015) Standard test methods for rockwell hardness of metallic materials. ASTM International, West Conshohocken, PA. https://doi.org/10.1520/E0018-15
37. Kruth JP, Mercelis P, Van Vaerenbergh J, Froyen L, Rombouts M (2005) Binding mechanisms in selective laser sintering and selective laser melting. Rapid Prototyp J 11:26–36
38. Lu Y et al (2015) Investigation on the microstructure, mechanical property and corrosion behavior of the selective laser melted

CoCrW alloy for dental application. Mater Sci Eng C 49:517–525. https://doi.org/10.1016/j.msec.2015.01.023
39. Casalino G, Campanelli SL, Contuzzi N, Ludovico AD (2015) Experimental investigation and statistical optimisation of the selective laser melting process of a maraging steel. Opt Laser Technol 65:151–158. https://doi.org/10.1016/j.optlastec.2014.07.021
40. Kruth J-P, Badrossamay M, Yasa E, Deckers J, Thijs L, Van Humbeeck J (2010) Part and material properties in selective laser melting of metals. In: Proceedings of the 16th international symposium on electromachining, pp 1–12
41. Singh A, Datta S, Mahapatra SS, Singha T, Majumdar G (2013) Optimization of bead geometry of submerged arc weld using fuzzy based desirability function approach. J Intell Manuf 24(1):35–44